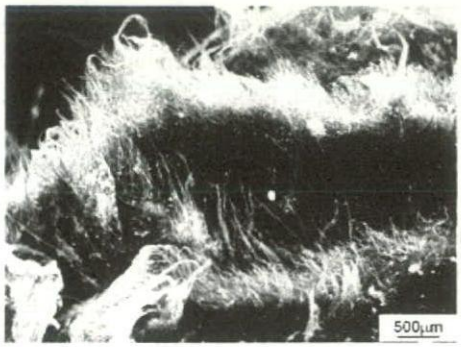

Fig. 13 SEM image of fracture surface of the SWCNT solid. (Processing condition: 1200°C, 120 MPa)

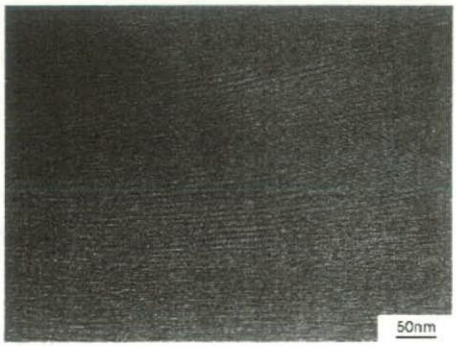

Fig. 14 TEM image of the SWCNT solid. (Processing condition: 600°C, 120 MPa)

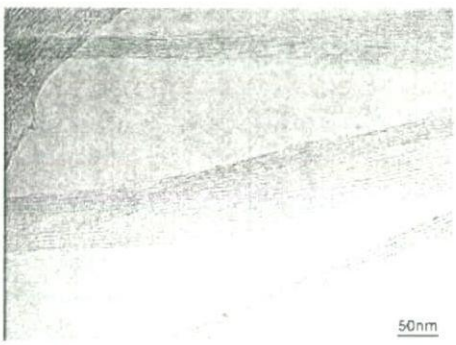

Fig. 15 TEM image of fracture surface of the SWCNT solid. (Processing condition: 600°C, 120 MPa)

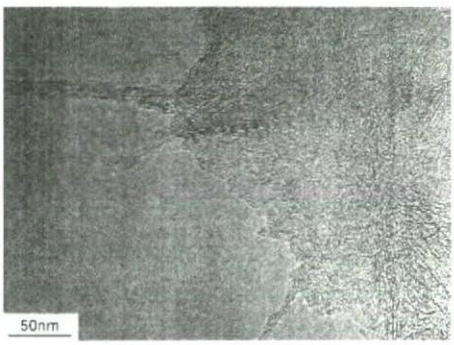

Fig. 16 TEM image of fracture surface of the SWCNT solid. (Processing condition: 1400°C, 120 MPa)

low-temperature treated solids. It is noted that SWCNT bundles are embedded in the amorphous-like structure, which is transformed from SWCNTs. The tighter links between the SWCNTs and amorphous-like structure may cause the improved mechanical properties that occur when the materials are prepared at higher sintering temperatures.

4. Summary

In this study, the SPS method was employed to solidify SWCNTs only, and the effects of processing conditions on the mechanical properties of the SWCNT solids were examined using the SP testing method. The sintering temperature used was in the range of 600~1400°C, and the sintering pressure used was 40MPa and 120 MPa. The obtained results can be summarized as follows:

(1) SWCNTs were successfully solidified without any additives by SPS.

(2) Purification of raw soot was critically important in order to improve the mechanical properties of the SWCNT solid, which exhibited a significant nonlinear deformation response in contrast with brittle fracture of the raw soot solid. The work of fracture of the SWCNT solids was 12.4 times larger than that of the raw soot solids.

(3) The Young's modulus and work of fracture of the SWCNT solids increased with the increasing sintering temperature and pressure, probably reflecting the improvement of interfacial strength between SWCNTs and amorphous-like structure transformed from SWCNTs caused by the spark plasma generated in the SPS process.

(4) The failure in the SWCNT solids occurred via intra-bundle sliding between SWCNTs, within and between the bundles.

Acknowledgments

This work was supported by the 21st Century COE Program Grant of the International COE of Flow Dynamics, and the Japan Ministry of Health, Labor and Welfare under Grants-in-Aid for Research on Advanced Medical Technology, which was supported by Ministry of Education, Culture, Sports, Science and Technology. We thank Mr. K. Motomiya of Graduate School of Engineering, Tohoku University for his technical assistance in TEM analysis.

References

(1) Iijima, S. and Ichihashi, T., Single-shell carbon nanotubes of 1-nm diameter, *Nature*, Vol. 363 (1993), pp. 603-605.

(2) Hamada, N. et al., New one-dimensional conductors: Graphitic microtubules, *Physical Review Letters*, Vol. 68, No. 8 (1992), pp. 1579-1581.

(3) Li, F. et al., Tensile strength of single-walled carbon nanotubes directly measured from their macroscopic ropes, *Applied Physics Letters*, Vol. 77, No. 20 (2000), pp. 3161-3163.

(4) Yu, M.F. et al., Tensile loading of ropes of single wall carbon nanotubes and their mechanical properties, *Physical Review Letters*, Vol. 84, No. 24 (2000), pp. 5552-5555.

(5) Yakobson, B.I. et al., Nanomechanics of carbon tubes: Instabilities beyond linear response, *Physical Review Letters*, Vol. 76, No. 14 (1996), pp. 2511-2514.

(6) Zhan, G.D. et al., Single-wall carbon nanotubes as attractive toughening agents in alumina-based nanocomposites, *Nature Materials*, Vol. 2, No. 1 (2003), pp. 38-42.

(7) Ren, Y. et al., Tension-tension fatigue behavior of unidirectional single-walled carbon nanotube reinforced epoxy composite, *Carbon*, Vol. 41, No. 11 (2003), pp. 2177-2179.

(8) Omori, M., Sintering, consolidation, reaction and crystal growth by the spark plasma system (SPS), *Materials Science and Engineering A-Structural Materials Properties Microstructure and Processing*, Vol. 287, No. 2 (2000), pp. 183-188.

(9) Okuda, S. et al., Small punch testing method for the development of functionally gradient materials, *Transaction of the Japan Society of Mechanical Engineers A*, Vol. 57 (1991), pp. 940-945.

(10) Seraphin, S. and Zhou, D., Single-walled carbon nanotubes produced at high-yield by mixed catalysts, *Applied Physics Letters*, Vol. 64, No. 16 (1994), pp. 2087-2089.

(11) Kasuya, A. et al., Evidence for size-dependent discrete dispersions in single-wall nanotubes, *Physical Review Letters*, Vol. 78, No. 23 (1997), pp. 4434-4437.

(12) Yamamoto, G. et al., Effect of impurities on mechanical properties of SWNT solids prepared by spark plasma sintering, *Proceeding of the 15th Symposium on Functionally Graded materials*, (2003-11), pp. 157-162.

(13) Saito, Y. and Bandow, S., *Introduction to Carbon Nanotube*, (1998), pp. 194-198, CORONA PUBLISHING.

(14) Chesnokov, S.A. et al., Mechanical energy storage in carbon nanotube springs, *Physical Review Letters*, Vol. 82, No. 2 (1999), pp. 343-346.

Journal of
Nanoscience and Nanotechnology
Vol. 7, 2690–2695, 2007

Concentrated Colloids of Silica-Encapsulated Gold Nanoparticles: Colloidal Stability, Cytotoxicity, and X-ray Absorption

Yeon-Su Park[1,*], Atsuo Kasuya[1,*], Andriy Dmytruk[1], Noda Yasuto[1], Motohiro Takeda[2], Noriaki Ohuchi[3], Yoshinori Sato[4], Kazuyuki Tohji[4], Motohiro Uo[5], and Fumio Watari[5]

[1] *Center for Interdisciplinary Research, Tohoku University, Aoba-ku, Sendai 980-8578, Japan*
[2] *Department of Bioengineering and Robotics, Tohoku University, Aoba-ku, Sendai 980-8579, Japan*
[3] *Division of Surgical Oncology, Graduate School of Medicine, Tohoku University, Aoba-ku, Sendai 980-8574, Japan*
[4] *Graduate School of Environmental Studies, Tohoku University, Aoba-ku, Sendai 980-8579, Japan*
[5] *Graduate School of Dental Medicine, Hokkaido University, Kita-ku, Sapporo 060-8589, Japan*

As an effort to develop a new, effective, nontoxic X-ray contrast agent, the concentrated colloids of silica-encapsulated gold nanoparticles (Au@SiO_2 NPs) were fabricated and their colloidal stability, cytotoxicity, and X-ray absorption were investigated. The concentrated colloidal NPs were manufactured by forming a 4 nm-thick silica shell on the surface of each Au NP with 15 nm diameter, followed by enrichment to [Au] = 100 mM. They were very stable in water: the NPs were well separated each other without forming agglomerates and their optical property was very similar to that before enrichment. The colloidal stability of the NPs in biological environment was strongly dependent on their previous morphology in water. The NPs with minor shell damage were stable in phosphate buffered saline (PBS) solution: both in water and in PBS solution, they showed very similar morphology and optical property. However, the NPs with profound shell damage formed big agglomerates in PBS solution, resulting in the red-shift and broadening of the Au surface plasmon resonance peak. Cell viability and proliferation assessments revealed the biocompatibility of the Au@SiO_2 NPs: no apparent cytotoxicity was observed even at 100 ppm NPs. The concentrated colloidal NPs showed very strong X-ray absorption. Their relative X-ray transmittance to water was comparable to that of a commercial agent. Considering these, the concentrated colloids of the Au@SiO_2 NPs are suitable for an X-ray contrast agent.

Keywords: Gold, Silica, X-ray Absorption, Cytotoxicity, Colloidal Stability.

1. INTRODUCTION

As concerns on human health increase tremendously in modern society, there have been strong demands for more effective and safer medical diagnoses. One of the most indispensable modern diagnostic tools is a computed tomography (CT), which strongly relies on the contrast ability of X-ray contrast agents. Currently, tri-iodobenzene derivatives are extensively used as the contrast agents. However, sometimes these iodine-containing small organic molecules cause some serious problems such as limited imaging time, due to their short vascular circulation time, and renal toxicity. Thus, CT practices occasionally require intra-arterial catheterization which may impose serious health risks. In these regards, there have been ceaseless efforts to develop more effective and safer X-ray contrast agents.[1–5] Most of them have focused on the modification of iodine-containing contrast molecules: encapsulation in[1–4] or linkage to[5] biocompatible organic molecules/polymers. A recent report by Hainfeld et al., however, demonstrated a possibility of Au NPs for an X-ray contrast agent.[6] They obtained the contrast images of the blood vessels and some organs of mice, by utilizing concentrated colloids of 1.9 nm diameter Au NPs as an X-ray contrast agent.

The nontoxic nature of bulk Au and relatively large (e.g., a few nm or bigger in diameter) Au NPs has been well documented,[7,8] but investigations on the toxicity of small Au NPs have been scarce. Recently, Schmit et al. reported the toxicity of very small Au NPs.[9,10] The authors observed strong cytotoxicity from 1.4 nm Au NPs, of which size is in a range for deteriorative interaction with

*Authors to whom correspondence should be addressed.

1533-4880/2007/7/2690/006 doi:10.1166/jnn.2007.601

the major grooves of deoxyribonucleic acids (DNAs). Thus, for medical applications, it is highly desirable to use the Au NPs larger than DNA grooves (typically less than 2 nm). In addition to the cytotoxicity problem, the Au NPs commensurate with or smaller may cause poor X-ray contrast because of their short vascular circulation time. However, very large Au NPs are also undesirable for medical applications because of the colloidal stability of the NPs decreasing with size and the difficulty in preparing homogeneous large (e.g., 40 nm or bigger in diameter) Au NPs.[11] Taking these into account, relatively large (here, between 10 and 40 nm in diameter) Au NPs seem to be suitable for an X-ray contrast agent application.

Like many medical applications of other colloidal NPs, the application of colloidal Au NPs for an X-ray contrast agent requires them being in a highly concentrated state to ensure high X-ray contrast. However, it is not a trifle to prepare stable and concentrated colloids of relatively large Au NPs, without proper surface modifications, because of their strong tendency to coagulate in concentrated state. One of the most useful and bio-friendly surface modifications is to encapsulate each Au NP in a silica shell because silica is biocompatible, feasible for further surface modifications,[8,12–14] and has strong negative charge in biological environment.[15] The strong negative charge on the silica surfaces, contributing to electrostatic repulsion among the NPs, may enable to prepare highly stable and concentrated colloids of relatively large Au NPs.

There has been sparse documentation[16] on the concentrated colloids of silica-encapsulated Au ($Au@SiO_2$) NPs, even though plenty of documents[12,17–22] have been available on the morphology and optical property of the NPs and their assemblies prepared from relatively low precursor concentration without enrichment. Unfortunately, no documentation is available on the colloidal stability and cytotoxicity of $Au@SiO_2$ NPs in biological environment, which are essential factors for medical applications. Here, as an effort to develop a new class of an effective and safe X-ray contrast agent, we report the colloidal stability in biological environment, *in vitro* cytotoxicity, and X-ray absorption of the concentrated colloidal $Au@SiO_2$ NPs (Au core diameter = ca. 15 nm, silica shell thickness = ca. 4 nm), along with their morphology and optical property.

2. EXPERIMENTAL DETAILS

2.1. Materials

Hydrogen tetrachloroaurate(III) tetrahydrate ($HAuCl_4 \cdot 4H_2O$), trisodium citrate dehydrate (Na_3-Cit), formaldehyde, 0.1 M phosphate buffered saline (PBS) solution were purchased from Wako Pure Chemicals. 3-Aminopropyl trimethoxysilane (APS) was supplied by Alfa-Aesar. Sodium silicate solution (ca. 27% SiO_2), DOWEX® 50WX4-400 ion-exchange resin, alpha-Minimum Essential Medium (MEM), and fetal bovine serum (FBS) were acquired from Sigma-Aldrich. Trypan blue and alamarBlue™ were provided by Gibco and Biosource, respectively. All chemicals were used as received. Milli-Q water (>18.2 MΩ cm) was used to prepare all aqueous solutions.

2.2. Preparation

The colloids of citrate-stabilized Au NPs were prepared according to the previously reported procedure.[11,16] Briefly, 15 ml of mildly heated 1% Na_3-Cit solution was added to 282 ml of boiling 0.532 mM $HAuCl_4 \cdot 4H_2O$ solution under stirring: the final concentrations of Au^{3+} and citrate$^-$ were 0.5 and 0.17 mM, respectively. Silica shells were formed by adding 0.75 ml of 1 mM APS solution and 12 ml of 0.54 wt% sodium silicate solution (pH = 10.5–11, adjusted by using DOWEX® 50WX4-400 ion-exchange resin) to 300 ml of the colloids of citrate-stabilized Au NPs, followed by standing the mixtures (pH ≅ 8.5) for three days.[14,16,17,21] The resulting colloids of $Au@SiO_2$ NPs were cleaned by a series of washing cycle: centrifugation (25,000 × g, 15 minutes), supernatant removal, and redispersion in water. Concentrated colloids were prepared by repeating the washing cycle, while gradually decreasing the amount of water for redispersion in each cycle (hereafter, referred as a 'mild enrichment'). A typical mild enrichment consisted of 4 washing cycles. Assuming that all Au^{3+} ions were used for producing Au NPs, the concentration of metallic Au in the concentrated colloids was 100 mM, 200 times higher than that in the colloids before the enrichment. Twice repetition of the mild enrichment was also performed to investigate its influence on the morphology and optical properties of the NPs. In this case, the final concentration of metallic Au in the resulting colloidal solution was also adjusted to 100 mM. For convenience, the metallic Au concentration was used for representing the concentration of Au or $Au@SiO_2$ NPs in colloids.

2.3. Instrument and Characterization

For characterizing the morphology of the NPs, the transmission electron microscopy (TEM) was performed with a JEOL JEM-2000 microscope operating at 200 KeV. The optical property of the colloidal NPs was characterized from their visible absorption spectra obtained with a Hitach U-2000 spectrophotometer. All optical spectra were obtained after adjusting metallic Au concentration to 0.5 mM. A Rigaku Rotaflex X-ray spectrometer was used for measuring X-ray transmittances of samples.

The stability of the concentrated colloidal NPs in biological environment was characterized based on the changes in their morphology and optical property upon transferring to 0.1 M PBS solution. The volume ratio of the colloid to the PBS solution was set to 0.5.

The viability and proliferation of rat fibroblast MC3T3-E1 cells, assessed by using a almarBlue™ assay, were used for evaluating the cytotoxicity of the NPs. For cell viability tests, the rat fibroblasts were incubated at 37° in 24-well plates using alpha-MEM containing 10% FBS (10^4 cells per well) and then various amount of the NPs (0.01–100 ppm) in water were added to each well. After further incubation at 37° for 24 hours, the viability of the rat fibroblasts was estimated based on the calorimetric detection of almarBlue™ reduction caused by live cells. For cell proliferation assays, both the rat fibroblasts and the NPs in water were seeded onto 24-well plates using alpha-MEM containing 10% FBS (10^4 cells per well) and then co-incubated for 24 hours. After cell fixing with formaldehyde and staining with trypan blue, stained cells (live cells) were counted under an optical microscope. In both the tests, the control sample was rat fibroblast MC3T3-E1 cells.

3. RESULTS AND DISCUSSION

3.1. Morphology

The citrate-induced reduction of Au^{3+} produced homogeneous spherical Au NPs with ca. 15 nm in diameter (Fig. 1(a)). The $Au@SiO_2$ NPs, prepared through silica coating in the basic silicate solution, are well separated each other without forming agglomerates, as shown in Figure 1(b). They have relatively homogeneous spherical silica shells of which thickness is ca. 4 nm.

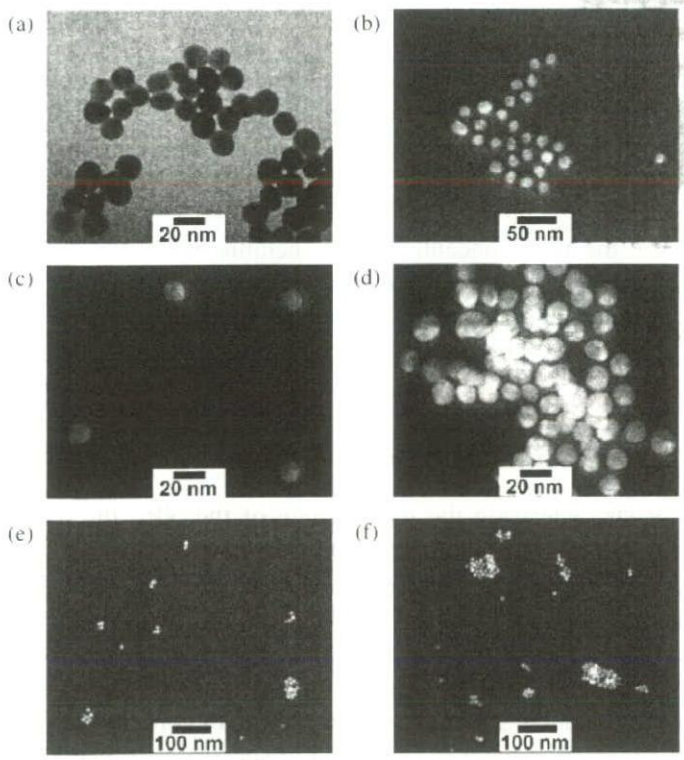

Fig. 1. TEM images of Au and $Au@SiO_2$ nanoparticles: (a) citrate-capped Au, (b) as-prepared $Au@SiO_2$ in water, (c) $Au@SiO_2$ in water after mild enrichment, (d) $Au@SiO_2$ after twice repetition of mild enrichment, (e) $Au@SiO_2$ in 0.1 M PBS solution after mild enrichment, and (f) $Au@SiO_2$ in 0.1 M PBS solution after twice repetition of mild enrichment. The concentrations of the NPs before and after the enrichments were equivalent to 0.5 and 100 mM metallic Au, respectively.

The concentrated colloidal $Au@SiO_2$ NPs, prepared through the mild enrichment, are well separated each other without forming agglomerates, even though some silica shells have minor shell damage such as detachment of some silica (Fig. 1(c)). The stability of these concentrated colloidal $Au@SiO_2$ NPs with minor shell damage (MSD) can be attributed to their high surface charge. In the experimental conditions of near neutral pH, the silica surfaces have high negative charge owing to the low isoelectric point of silica.[15] This enhances electrostatic repulsion among the NPs enough to stabilize them in the concentrated state.

The repetition of the mild enrichment exerted detrimental effect on the morphology of the $Au@SiO_2$ NPs. As shown in Figure 1(d), twice repetition of the enrichment resulted in profound shell damage (PSD): the silica shells seem to be inhomogeneous and little compact, compared with those obtained through the typical mild enrichment process; in part, they are loosely distributed among the Au NPs. Most of the NPs with PSD are poorly separated each other. In many cases, each NP is closely contacting with its immediate neighbor NPs through very thin silica barrier. Some NPs partially expose their Au cores or have big cores compose of two or more Au NPs. The formation of the big cores is related with the coagulation of the NPs with no or little silica. They have surface charge insufficient to prevent them from coagulation, because their surface charge diminishes with decreasing silica surface area.

3.2. Optical Property

As shown in Figures 2(a) and (b), the formation of 4 nm-thick silica shells caused a shift of Au surface plasmon resonance (SPR) peak from 519 to 523 nm. This red-shift by 4 nm is due to an increase in the local refractive index of the surrounding medium[17, 22] and is well in accordance with previous reports.[16, 17]

The optical property of the $Au@SiO_2$ NPs was strongly dependent on their morphology. As shown in Figure 2(c), the NPs with MSD show a SPR peak of which shape, intensity, and position are very similar to those of the NPs before the enrichment (Fig. 2(b)). The SPR peak of the NPs with PSD in Figure 2(d), however, is somewhat broad, weak, and red-shifted by 3 nm, compared with that of the NPs with MSD. These slight changes in optical property can be attributed to the close contact of the NPs and the existence of the NPs with bigger Au core.

3.3. Colloidal Stability in Biological Environment

In biological environment, the concentrated colloidal $Au@SiO_2$ NPs formed agglomerates of which size was strongly dependent on their initial morphology in water.

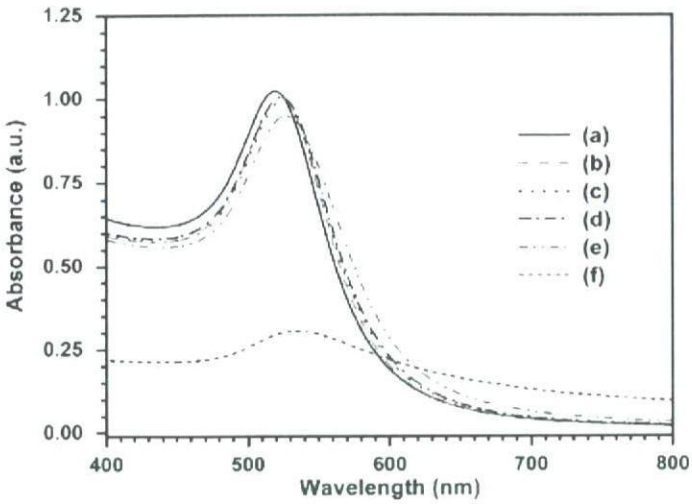

Fig. 2. Visible absorption spectra of Au and $Au@SiO_2$ nanoparticles: (a) citrate-capped Au, (b) as-prepared $Au@SiO_2$ in water, (c) $Au@SiO_2$ in water after mild enrichment, (d) $Au@SiO_2$ after twice repetition of mild enrichment, (e) $Au@SiO_2$ in 0.1 M PBS solution after mild enrichment, and (f) $Au@SiO_2$ in 0.1 M PBS solution after twice repetition of mild enrichment.

As shown in Figure 1(e), the morphology of the NPs with MSD in the PBS solution is very similar to that of the corresponding NPs in water, except for some agglomerates composed of relatively small number of the NPs. The formation of slightly more and bigger agglomerates of the NPs in the PBS solution is related with the flocculation caused by an increase in the ionic strength of the solution. Due to its high ion concentration, the PBS solution has stronger ionic strength than water. As the ionic strength of a solution increases, charge (opposite in sign) density around NPs increases. Because both ionic strength and charge density are inversely proportional to the square of the Debye shielding length, which is a measure of the strength of electrostatic potential damping from its pure value, electrostatic repulsion among the NPs is reduced and hence the NPs are destabilized with increasing ion concentration. Unlike those with MSD, the concentrated colloidal $Au@SiO_2$ NPs with PSD were unstable in the PBS solution: an immediate formation of precipitates was observed upon transferring to the solution. As shown in Figure 1(f), the TEM images of the NPs with PSD in the PBS solution show big agglomerates, along with some single NPs and small agglomerates composed of a few NPs with little or no silica shell. The big agglomerates consist of a few tens of the NPs, in which a couple of bigger Au NP cores are included. As discussed earlier, the formation of the big agglomerates of the NPs with PSD is related with the ionic strength of the PBS solution.

The optical property of the $Au@SiO_2$ NPs in PBS solution was also strongly influenced by their initial morphology: the NPs with MSD showed little change, whereas those with PSD experienced drastic change. The visible absorption spectrum of the NPs with MSD in the PBS solution (Fig. 2(e)) is very similar to that of the corresponding NPs in water (Fig. 2(c)): there is little difference in the shape, intensity, and position of the Au SPR peak. However, as shown in Figure 2(f), the NPs with PSD in the PBS solution shows a broad and weak Au SPR peak with very large background, compared with those in water (Fig. 2(d)). And their SPR peak is located at 534 nm, which is 7 nm longer than that in water. These optical observations imply the existence of various sizes of bigger NPs in the PBS solution and are well coincided with the previously described microscopic observations.

3.4. Cytotoxity

For medical applications, the $Au@SiO_2$ NPs should be biocompatible. Their biocompatibility was evaluated based on the viability and proliferation of rat fibroblast MC3T3-E1 cells. In general, 50% cell viability (or proliferation) is considered as a border of live or dead cells: materials giving 50% or higher cell viability (or proliferation) are biocompatible, while those with lower than 50% values are toxic. Figure 3 shows the viability and proliferation of the rat fibroblast cells after 24 hours incubation. In all the NP concentrations tested here, the rat fibroblast cells show more than 50% viability and proliferation. Even at a very high NP concentration of 100 ppm, the cell viability and proliferation are more than 70 and 60%, respectively. These confirm the biocompatibility of the $Au@SiO_2$ NPs. Especially the NPs show excellent biocompatibility at the concentration of 1 ppm or lower, as can be inferred from near 100% cell viability and proliferation.

3.5. X-ray Absorption

For achieving high X-ray contrast, contrast agents should show much stronger X-ray absorption (so, much lower X-ray transmittance) than human body, because X-ray contrasting ability relies on the differences in their X-ray

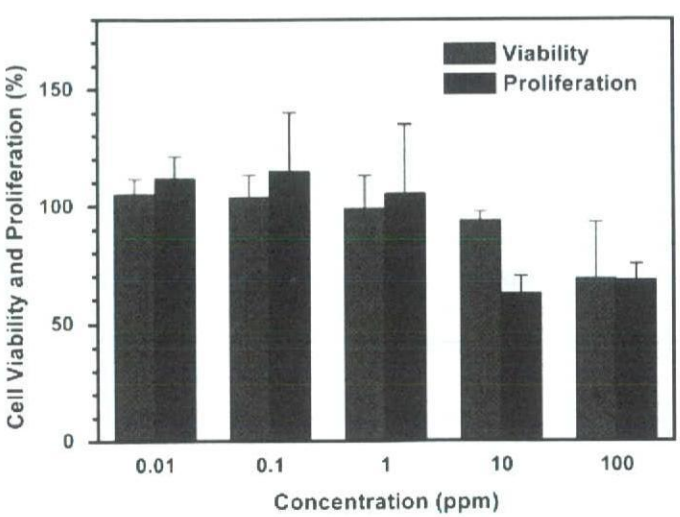

Fig. 3. Viability and proliferation of rat fibroblast MC3T3-E1 cells at various concentrations of $Au@SiO_2$ nanoparticles.

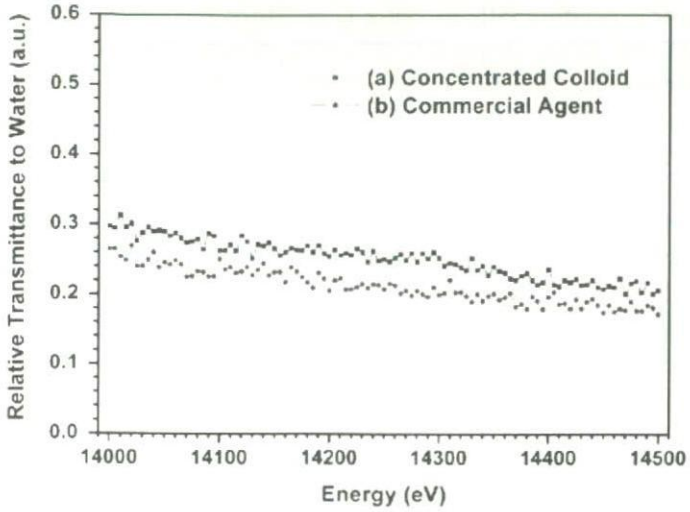

Fig. 4. Relative X-ray transmittances of (a) the concentrated colloid of $Au@SiO_2$ nanoparticles ([Au] = 100 mM) and (b) a commercial X-ray contrast agent (Iopamiron® 300). Relative transmittance = transmittance of sample/transmittance of water.

absorption. Therefore, the relative X-ray transmittance of a sample to water (a major constituent of human body) is a very important factor for evaluating its contrast ability. In general, materials with lower relative X-ray transmittance give better X-ray contrast.

Figure 4 shows the relative X-ray transmittances of the 100 mM colloidal $Au@SiO_2$ NPs and a commercial X-ray contrast agent (Iopamiron® 300). Average relative transmittance of the colloidal NPs is close to that of the commercial contrast agent. At Au L_1 edge, the colloidal NPs shows the relative transmittance of ca. 0.237, which is very close to the calculated value of 0.231 based on X-ray mass attenuation coefficient of Au. Their slight discrepancy may be mainly due to the loss of the NPs during enrichments. Considering very low relative X-ray transmittance, comparable to that of a commercial contrast agent, the concentrated colloidal $Au@SiO_2$ NPs may be suitable for an X-ray contrast agent application.

4. SUMMARY AND CONCLUSIONS

As an effort to develop a new class of an effective and nontoxic X-ray contrast agent, highly concentrated colloidal $Au@SiO_2$ NPs were prepared and their colloidal stability in biological environment, *in vitro* cytotoxicity, and X-ray absorption were investigated. Each NP consists of ca. 15 nm diameter Au core and ca. 4 nm thick silica shell. The concentration of the concentrated colloidal NPs was equivalent to 100 mM metallic Au.

Highly stable and concentrated colloidal $Au@SiO_2$ NPs with MSD were prepared through the mild enrichment. The colloidal NPs with MSD were morphologically stable in concentrated state: they were well-separated each other, without forming agglomerates. The optical property of the concentrated colloidal NPs with MSD was very similar to that of the colloidal NPs before the enrichment: there was little change in the shape, intensity, and position of Au SPR peaks before and after the enrichment.

The concentrated colloidal $Au@SiO_2$ NPs with PSD were prepared through the repetition of the mild enrichment. The concentrated colloidal NPs with PSD showed the morphology somewhat different from that of the concentrated colloidal NPs with MSD: they were poorly separated each other and had very close contact with neighbor NPs. Due to their morphology, the NPs with PSD showed a Au SPR peak which is slightly broad, weak, and red-shifted as compared with that of the NPs with MSD.

In biological environment, the stability of the concentrated colloidal $Au@SiO_2$ NPs was strongly dependent on their previous morphology in water. The concentrated colloidal NPs with MSD were stable in PBS solution, even though some small agglomerates were formed. However, the concentrated colloidal NPs with PSD were unstable in PBS solution: they formed big agglomerates, resulting in precipitation. These morphological differences affected their optical property. The colloidal NPs with MSD in PBS solution showed the Au SPR peak similar to that of the NPs in water, whereas those with PSD showed a very broad and red-shifted peak in PBS solution, as compared with those in water.

The $Au@SiO_2$ NPs are biocompatible. Both cell viability and proliferation assessments revealed no apparent cytotoxicity of the NPs even at the highest NP concentration tested here (100 ppm). Especially, at 1 ppm or lower, the NPs have an excellent biocompatibility: they showed near 100% cell viability and proliferation.

The concentrated colloidal $Au@SiO_2$ NPs showed strong X-ray absorption. Their relative transmittance to water, being inversely proportional to their X-ray contrast ability, is very low and close to that of a commercial contrast agent.

Taking into account their high colloidal stability in biological environment, excellent biocompatibility, and relative X-ray transmittance comparable to a commercial agent, the concentrated colloids of the $Au@SiO_2$ NPs, with relatively large Au core and little (or no) silica shell damage, are excellent materials for X-ray contrast agents.

Acknowledgments: This work was partially supported by Grant-in-Aid from the Ministry of Education, Science, Sports, and Culture, Japan. Authors wish to thank Prof. M. Konno of Tohoku University for his generosity in using the centrifuge.

References and Notes

1. U. P. Schmiedl, W. Krause, J. Leike, and A. Sachse, *Acad. Radiol.* 6, 164 (**1999**).
2. V. P. Torchilin, *Adv. Drug Deliv. Rev.* 54, 235 (**2002**).
3. D. R. Vera and R. F. Mattrey, *Acad. Radiol.* 9, 784 (**2002**).
4. C.-Y. Kao, E. A. Hoffman, K. G. Beck, R. V. Bellamkonda, and A. V. Annapragada, *Acad. Radiol.* 10, 475 (**2003**).
5. V. P. Torchilin, M. D. Frank-Kamenetsky, and G. L. Wolf, *Acad. Radiol.* 6, 61 (**1999**).

6. J. F. Hainfeld, D. N. Slatkin, T. M. Focella, and H. M. Smilowitz, *Br. J. Radiol.* 79, 248 (**2006**).
7. E. E. Connor, J. Mwamuka, A. Gole, C. J. Murphy, and M. D. Wyatt, *Small* 1, 325 (**2005**).
8. Z. P. Xu, Q. H. Zeng, G. Q. Lu, and A. B. Yu, *Chem. Eng. Sci.* 61, 1027 (**2006**).
9. Y. Liu, W. Meyer-Zaika, S. Franzka, G. Schmid, M. Tsili, and H. Kuhn, *Angew. Chem., Int. Ed.* 42, 2853 (**2003**).
10. M. Tsoli, H. Kuhn, W. Brandau, H. Esche, and G. Schmid, *Small* 1, 841 (**2005**).
11. G. Frens, *Nat. Phys. Sci.* 241, 20 (**1973**).
12. E. Mine, A. Yamada, Y. Kobayashi, M. Konno, and L. M. Liz-Marzán, *J. Colloid Interf. Sci.* 264, 385 (**2003**).
13. T. Schiestel, H. Brunner, and G. E. M. Tovar, *J. Nanosci. Nanotechnol.* 4, 504 (**2004**).
14. B. Rodríguez-González, A. Sánchez-Iglesias, M. Giersig, and L. M. Liz-Marzán, *Faraday Discuss.* 125, 133 (**2004**).
15. X. Cui, W.-C. Zin, W.-J. Cho, and C.-S. Ha, *Mater. Lett.* 59, 2257 (**2005**).
16. Y.-S. Park, L. M. Liz-Marzán, A. Kasuya, Y. Kobayashi, D. Nagao, M. Konno, S. Mamykin, A. Dmytruk, M. Takeda, and N. Ohuchi, *J. Nanosci. Nanotechnol.* 6, 3503 (**2006**).
17. L. M. Liz-Marzán, M. Giersig, and P. Mulvaney, *Langmuir* 12, 4329 (**1996**).
18. F. Caruso, M. Spasova, V. Salgueiriño-Maceria, and L. M. Liz-Marzán, *Adv. Mater.* 13, 1090 (**2001**).
19. F. García-Santamaría, V. Salgueiriño-Maceria, C. López, and L. M. Liz-Marzán, *Langmuir* 18, 4519 (**2002**).
20. Y. Yang, M. Hori, T. Hayakawa, and M. Nogami, *Surf. Sci.* 579, 215 (**2005**).
21. I. Tunc, S. Suzer, M. A. Correa-Duarte, and L. M. Liz-Marzán, *J. Phys. Chem. B* 109, 7597 (**2005**).
22. S. Liu and M. Han, *Adv. Funct. Mater.* 15, 961 (**2005**).

Received: 25 October 2006. Revised/Accepted: 22 November 2006.

カーボンナノチューブの表面改質に関わる細胞毒性

Cytotoxicity concerning surface treatment of carbon nanotubes

佐藤 義倫　東北大学 大学院 環境科学研究科 環境科学専攻　助教

〒980-8579　宮城県仙台市青葉区荒巻字青葉 6-6-20，Tel 022-795-3868，Fax 022-795-3868，

E-mail：hige@bucky1.kankyo.tohoku.ac.jp

1 はじめに

悪性中皮種を発現するアスベスト[1]に形状が似ている繊維状のカーボンナノチューブ（Carbon Nanotubes: CNTs）[2]は毒性を示すのだろうか？細胞毒性を引き起こす要因には，金属溶出[3]，表面官能基[4,5]，比表面積，サイズ効果[6-9]が知られている。金属溶出は金属表面が体内の酸性により腐食し，イオンとして溶出することによって細胞に影響を与える（金属腐食）。細胞や組織内での金属腐食は最も知られた細胞毒性を引き起こす要因であり，金属のイオン化傾向に依存すると言われる。例えば，インプラント材料であるTi合金（Ti-6Al-4V）のAlはしばしば溶出し[10]，骨の成長阻害因子やアルツハイマー病の発症因子の原因として挙げられ[11]，またNiやVの溶出は強い細胞毒性を示す。Fe^{2+}は触媒作用を示し，過酸化水素からヒドロキシルラジカルや，過酸化脂質からアルコキシルラジカルを産出し，酸化性ストレスを誘導するという報告がある。さらに，磁性酸化鉄（Fe_3O_4）はアルツハイマー病，パーキンソン病などの神経退化性疾患と関連していると指摘されている[12-14]。表面官能基による毒性要因の例は，表面を覆う官能基の種類から由来する毒性である。細胞標識として注目されているCdSe量子ドットをCOOH/OHが混在した表面修飾したものは細胞毒性を示さず，COOHのみの表面修飾では細胞毒性を示すと報告されている[4]。一方，ナノ粒子の生体影響を考えるときに粒径が極めて小さくなると（サイズ依存性），ナノ粒子表面の物理的性質（高比表面積，表面電子状態の活性化），化学的性質と細胞との相互作用によるナノ粒子の体内挙動が問題となる。生体界面活性剤で被覆された金粒子は生体親和性があるが[5]，直径1.4 nmの金ナノ粒子は電子状態の変化により被覆された生体界面活性剤が外れ，DNAに吸着して安定化してしまう。この金ナノ粒子に吸着されたDNAは正常に働かず，毒性を引き起こす[9]。一般に生体親和性の高いテフロン[6]やTi[7,8]もナノサイズになると肺毒性，細胞毒性を示すことが知られている。一方，1970年代に米国のスタントン[15]と西ドイツのポット[16]は独自に繊維状形態に着目し，サイズ（長さ，直径）を調製した様々な物質をラットやマウスの胸腔，腹腔に注入し長期間飼育後，胸腔，腹腔の病変や悪性中皮種の発現率を調べている。その結果，生体内で耐久性があり，細くて長い繊維状物質は化学組成や結晶構造に関係なく発ガン性を持つことを示し，特に幅0.25 μm以下で，長さ8.0 μm以上の繊維の中皮種発現率が最も高いことを見出している。では，幾つの細胞毒性要因がCNTsに対して当てはまるのだろうか？

単層カーボンナノチューブ（single-walled carbon nanotubes；SWCNTs），多層カーボンナノチューブ（multi-walled carbon nanotubes；MWCNTs）は触媒金属を用いることにより合成される（アーク放電法で合成される多層CNTsを除く）。その触媒金属は，Fe，Co，Ni，Y，La，Ce，YNi，FeNi，CoNi，CoMo，MgO，Al_2O_3などと単体金属，合金，金属酸化物と数多く知ら

れている[17]。したがって，未精製のCNTsには金属粒子が含まれている場合がほとんどである。また，応用に応じて様々な機能性官能基を化学修飾することが可能であり，比表面積も大きい。さらに繊維状であり，直径，長さ，形態も様々である。このように，CNTsは金属溶出，表面官能基，比表面積，サイズ効果の細胞毒性を引き起こす要因を所有している。これらに加え，疎水性表面を持つCNTsは水溶液で凝集するため，凝集効果も毒性要因に加わる可能性があることも見逃してはならない。

異物が生体内に進入すると，貪食細胞（マクロファージや多核巨細胞）が異物を除去するために取り込む。その後，異物は食胞に取り囲まれ，リソソームと融合し，ファゴリソームを形成し，酵素により異物を低分子化する。低分子化された異物は無毒化され，排出される。貪食する際には，貪食細胞表面にあるレセプターにより異物を認識するが，その際にサイトカイン（種々の細胞から分泌されるホルモン様低分子蛋白の総称で，免疫反応の強さと期間を調節し細胞同士の情報交換を媒介する）を産出し，その量が毒性評価の1つになる。したがって，細胞毒性は材料と細胞との接触から誘発されるため，CNTsの表面と細胞の相互作用は重要となる。一方，医工学応用ではDNA，遺伝子の導入や形質移入のトランスポーターとしてCNTsの形状に強い関心が持たれている[18]。DNAのトランスポーターには，ウィルスベクター（レトロ，レンチ，アデノ）やカチオン脂質，ポリエチレニミン（PEI）[19]，カチオンポリマーを含む非ウィルス形質移入ベクターなどがある。これらのウィルスベクターは遺伝子の搬送を妨げる免疫反応を細胞から誘発することが多い。PEIや非ウィルス形質移入ベクターはこの問題を回避できるが，核膜浸透，遺伝子発現効率が低いことが問題となっている。いずれにせよ，トランスポーターは目的の細胞へ辿り着く前に貪食されず，かつ目的細胞へ潜り込む機能を持たせなくてはならない。CNTsのトランスポーターとして使用するには，CNTs表面への修飾を施すことになるが，施されたCNTsが毒性を示しては意味が無くなってしまう。

以上のことから，細胞とCNTs表面の接触が細胞毒性に大きく関わっているため，本稿ではCNTsの表面に関わる細胞毒性について最近の動向を報告する。

2 未化学修飾のCNTsの細胞毒性

Monteiro-Riviereらは[20]，ヒト表皮細胞に対して竹の子構造を持つMWCNTs（CVD法）の影響を生体外（in vitro）試験により調べている。MWCNTsは培養液に0.1，0.2，0.4 mg/mLの濃度に調製し，ヒト由来の表皮細胞と混合し24時間培養した。MWCNTsはサイトカインであるIL-8（インターロイキン8；急性期炎症反応における好中球遊走，活性化にかかわる本質的な因子）を誘発し，細胞生存率が減少することを時間依存性，濃度依存性試験から確認している。さらに透過型電子顕微鏡（transmission electron microscope；TEM）からは，表皮細胞内にMWCNTsが存在することも観察された（図1）。つまり，MWCNTsは貪食されていたことになる。このことから，ヒト表皮細胞に対してMWCNTsは毒性を示すと考察している。

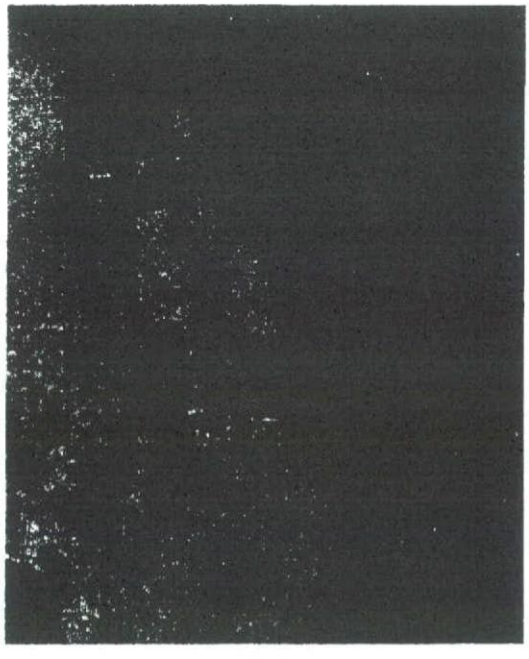

図1　表皮細胞の小胞内の透過型電子顕微鏡写真，矢印で示されている物質が竹の子状のMWCNTs[20]

Mullerらは[21]，「精製MWCNTs」と「精製MWCNTsの粉砕物」を調製し，20，50，100 μg/mLの濃度を腹膜マクロファージ（マクロファージ；異物を貪食する

貪食細胞）を用いて2ヶ月間生体外試験（*in vitro*）を行っている。細胞毒性は乳酸脱水素酵素放出（培養24時間後），炎症性は培養6時間後の腫瘍壊死因子（tumor necrosis factor- α；TNF- α）である腫瘍細胞を壊死させる作用のある物質を測定して評価している。彼らは精製MWCNTsの粉砕物はアスベストやカーボンブラックと同様な濃度依存性を示す毒性があるが，精製MWCNTsにおけるTNF- α量や炎症は精製MWCNTsの粉砕物のものと比較すると低く，重大な毒性を示さないと言及している。「精製MWCNTsの粉砕物」は瑪瑙ボールミルでサンプルを調製しており，瑪瑙の磨耗物がサンプルに混入している可能性がある。瑪瑙は微結晶質石英の集合体であり，結晶質シリカは高い発ガン性物質として位置付けられているため[22]，粉砕で混入した瑪瑙の磨耗物の影響が現れている可能性も考えられる。

Koyamaらは[23]，4つの異なる精製されたCNTs（SWCNTs，直径の異なるMWCNTs，カップ型MWCNTs）を末梢血中T細胞の$CD4^+$と$CD8^+$の測定，また皮下細胞に埋入した時の周囲軟組織の炎症反応（3ヶ月間）を病理組織学的に調べているが，アスベストと比較すると格段に低く，急性の細胞毒性は示していない。

3 化学修飾のCNTsの細胞毒性

Sayesらは[24]，*in vitro*でヒト由来真皮線維芽細胞を使用し，SWCNTsの細胞毒性における官能基の化学修飾度の影響を調べている。SWCNTsは SWCNT-phenyl-SO_3H，SWCNT-phenyl-SO_3Na（SWCNTsに対する-phenyl-SO_3Xの化学修飾度はC/CF = 18，41，80。C/CFは化学修飾されているSWCNTsの炭素原子に対するSWCNTsの全炭素原子の割合を示し，数値が低いほど化学修飾度が高い），SWCNT-phenyl-$(COOH)_2$（SWCNTsに対する-phenyl-$(COOH)_2$の修飾度はC/CF = 23），1.0％プルロニックF108被覆したSWCNTsを使用している。SWCNTsの化学修飾度が増加すると，界面活性剤で被覆したSWCNTsよりも大幅に細胞毒性が低いことを見出している（図2）。化学修飾されたSWCNTsの細胞生存率は50％未満にはならない。

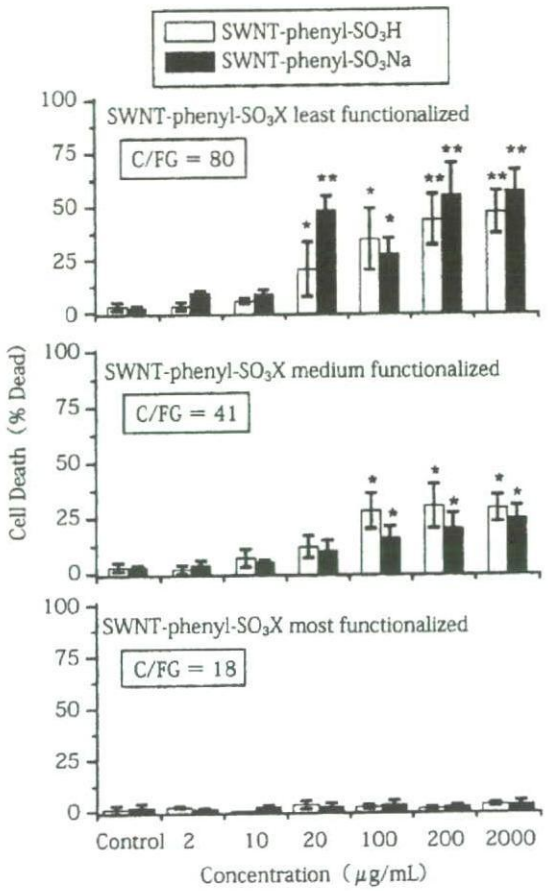

図2 SWCNT-phenyl-SO_3H（□）とSWCNT-phenyl-SO_3Na（■）の濃度に対する細胞活性率。SWCNTsに対する-phenyl-SO_3Xの化学修飾度はC/CF = 80（上段），41（中段），18（下段）である。C/CFは化学修飾されているSWCNTsの炭素原子に対するSWCNTsの全炭素原子の割合を示し，数値が低いほど化学修飾度が高いことを示している[24]

CNTsをナノサイズの移動媒体として医工学応用するために，Luらは[25]，SWCNTs /RNAポリマー・ポリ（rU）複合体（ポリ（rU）の塩基類は，SWCNTsベーサル面の炭素環によるπ－積層も形成可能であり，SWCNTsとRNAポリマー・ポリ（rU）の疎水性窒素性塩基類がSWCNTsのベーサル面との物理的な結合していると推測している）のMCF乳がん細胞への搬送実験を行なった。SWCNTs /RNAポリマー・ポリ（rU）複合体の可視化はヨウ化プロピジウム（PI）を塩基対間に挿入させ，共焦蛍光顕微鏡で観測している。この実験か

ら，SWCNTs /RNA ポリマー・ポリ（rU）複合体は細胞膜，核膜を通過することを見出している。さらに MTS (3-(4,5- ジメチルチアゾール) 5-(3- カルボキシメトキシフェニル)-2-(4- スルホフェニル)-2- テトラゾリウム) アッセイの結果では，1.0 mg/mL 以下の濃度では MCF 乳がん細胞および表皮細胞のいずれに対する細胞毒性も示されていない。

Bianco らは[26,27]，化学修飾した SWCNTs，MWCNTs の生体親和性を報告している。^{111}In ラベルしたジエチレントリアミン五酢酸を化学修飾した SWCNTs を静脈内投与し，ガンマシンチグラフィーで観察している。TEM で排出された尿中に SWCNTs，MWCNTs が観察されたことから（図 3），化学修飾した SWCNTs，MWCNTs は肝臓や脾臓などの網内系臓器には蓄積せず，血液循環から腎排泄を通り，尿として排出されることを推定している[25]。一方，*in vitro* において，化学修飾した SWCNTs をマクロファージ，B リンパ球（B 細胞），T リンパ球（T 細胞）に取り込まれているが，細胞生存率には影響はなかった。溶解度の高い化学修飾した SWCNTs はそれぞれの免疫系細胞の機能は正常に保ったままであり，やや溶解度の低い化学修飾した SWCNTs は，マクロファージによる炎症性サイトカインの分泌を引き起こしてはいるものの，リンパ球の機能が保たれていることを確認している[26]。さらに，Bianco らは[28]，様々な種類の分子官能基（図 4）を修飾した SWCNTs，MWCNTs が繊維芽細胞，接着性細胞，菌細胞，酵母菌，バクテリアに取り込まれることを示した。図 5 は f-SWNT 1（SWNT-NH_3^+）と A549（肺上皮細胞）を 37℃，2 時間培養した後に，核，細胞膜を青，赤で蛍光染色したものを共焦点蛍光顕微鏡で観察したものである。緑は f-SWNT 1 にラベルされている蛍光色素である（a は SWCNTs のないコントロール）。このことからも核の近傍に CNTs が取り込まれていることがわかる。エンドサイトーシス（細胞外環境から細胞膜によって形成された小胞を介する物質の内在化）による細胞内への取り込みであるかを調べるために，アジ化ナトリウム（NaN_3）を用いたエンドサイトーシス抑制試験が試みられているが，抑制に無関係に SWCNTs は細胞内に取り込まれた。結局，化学修飾 CNTs は官能基の種類に関係なく，様々な種類の細胞壁を通り抜けることができるが，その取り込む機構は単純な ATP の加水分解で得られるエネルギーから得られる運動によるものと断定できず，エネルギー以外の機構で取り込まれている可能性を示している。その細胞膜進入機構の 1 つとして，大きな縦横比を持つシリンダー形状が細胞膜を進入，貫通できるのではないかと推測している。

化学修飾された CNTs は生体親和性に優れている結果を示しているが，これは官能基と細胞の親和性が高いためであると推測はできる。一方，未化学修飾の CNTs は現在のところ明快な結論は得られていない。CNTs のベーサル面のπ電子と細胞表面にあるレセプターとの相互作用によるシグナル伝達があるのであれば，何らかの細胞組織反応が現れるはずである。今後ベーサル面のπ電子と細胞表面にあるレセプターとのシグナル伝達の有無は明らかにしなければならない課題の 1 つである。

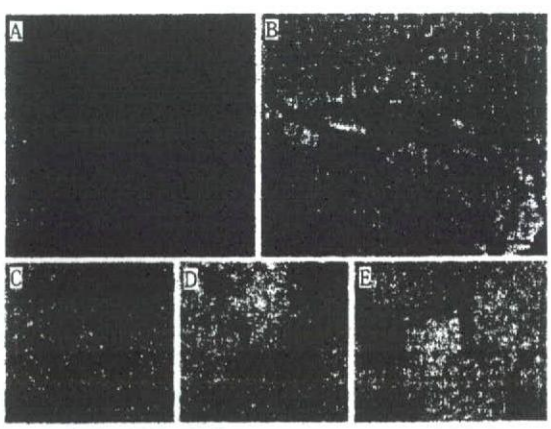

図 3　排出された尿の中の ^{111}In ラベルしたジエチレントリアミン五酢酸を化学修飾した SWCNTs（A，B スケールバー：500 nm）と MWCNTs（C，D，E スケールバー：100 nm）の透過型電子顕微鏡写真[26]

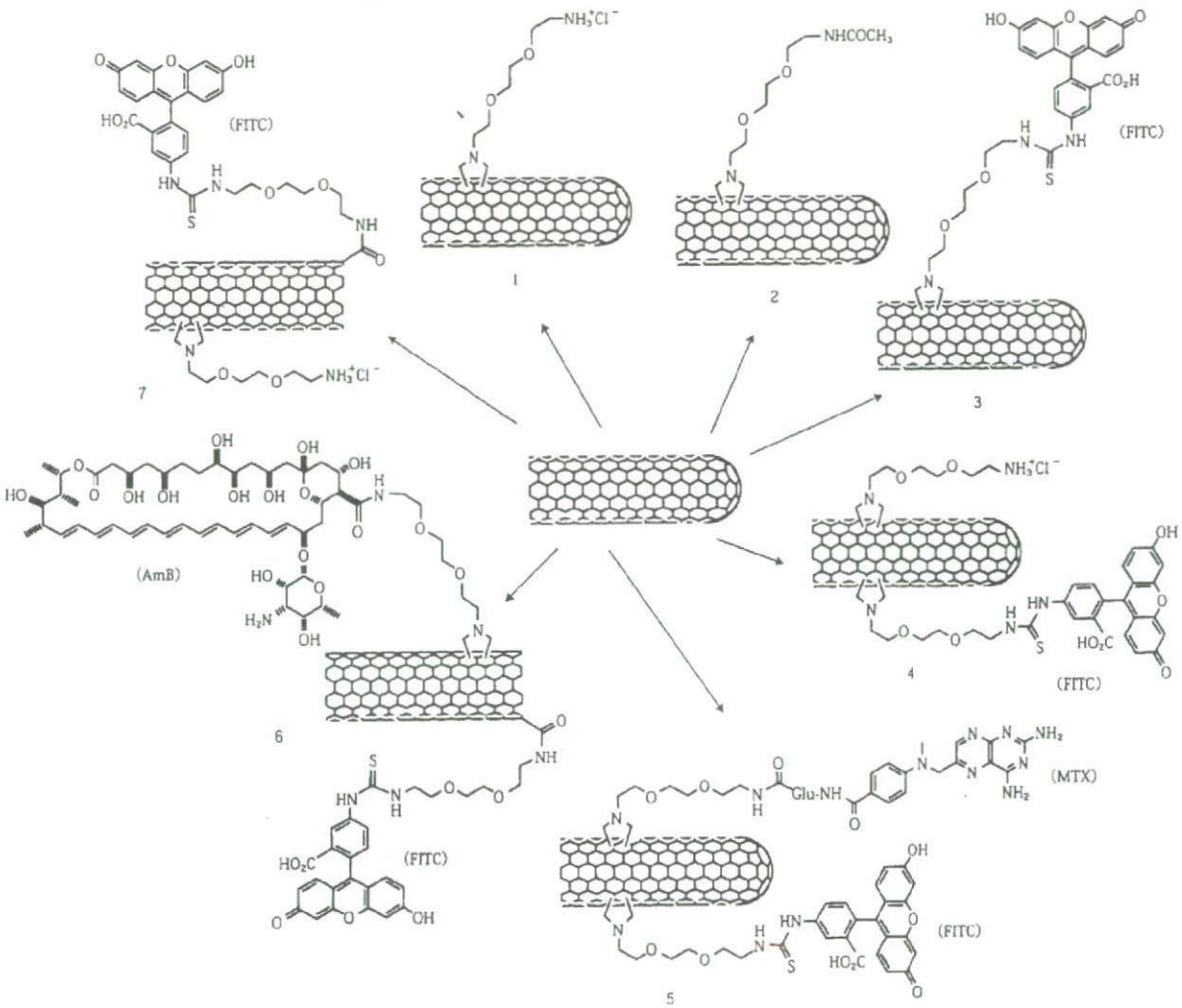

図 4　CNTs に共有結合させた様々な種類の分子官能基（文献 28）

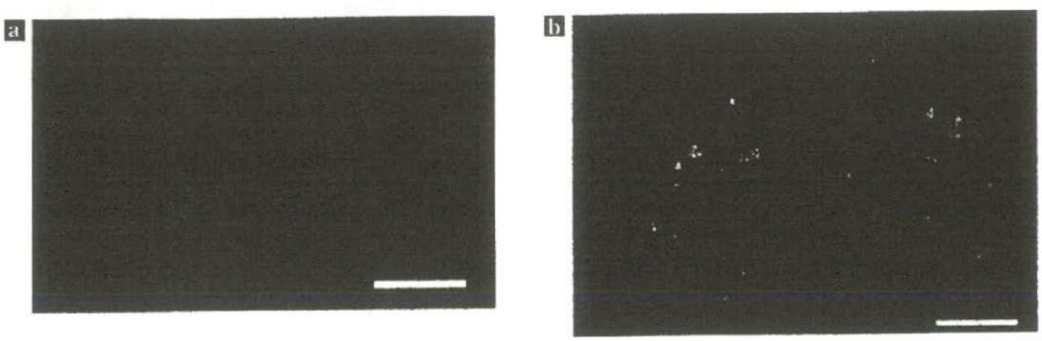

図 5　SWNT-NH_3^+と A549（肺上皮細胞）を 37℃，2 時間培養後に，核，細胞膜をそれぞれ青，赤で蛍光染色した共焦点蛍光顕微鏡写真。蛍光色素でラベルされた SWNT-NH_3^+は緑色の蛍光を発する。(a) SWNT 無し（コントロール），(b) SWNT-NH_3^+あり。スケールバー：20 μm[28]

4 CNTsのリスク評価法は正しいか？

毒性試験方法には大きく4つある。1つ目は対象物を加えた状態で所定期間細胞培養し，生存細胞数を顕微鏡で数える方法である。2つ目は細胞の代謝作用を利用するものである。細胞が生存していれば，細胞の代謝作用により外部の物質を取り込んで，細胞内の酵素作用によって化学変化を与える。それを利用して代謝されやすい色素を培地に加えて，吸収（又は蛍光）スペクトルの変化から細胞活性を求める方法である。3つ目は，細胞が刺激を受けたときに放出する細胞間のシグナル伝達物質などを測定する方法であり，この方法では細胞が破壊されるような強い毒性だけでなく，その前段階の刺激性を評価することも可能である。4つ目は，生体内（*in vivo*）での細胞・組織反応試験であり，異物が生体内でどのような挙動を示すのかの知見を得るためには，*in vivo* による試験は必須である。これまで，多くのCNTsは*in vitro* 方法によりナノ材料のリスク評価が行われてきた。しかし，CNTsになると，比表面積の増大による表面状態の影響が全く無いとは言い切ることはできず，従来のアッセイが適応できない可能性もある。

Wörle-Knirschらは[29]，SWCNTsの毒性をMTTアッセイにより評価している。MTTとはテトラゾリウム塩の一種 3-[4,5-dimethylthiazol-2-yl]-2,5-diphenyltetrazolium bromideであるが（水溶性で黄色の溶液），MTTが細胞内に取り込まれると細胞内のミトコンドリアにある脱水素によってホルマザンに変化する。このホルマザンは青色の非水溶性の結晶で生成後は沈殿するが，ジメチルスルホキシドで溶解させると赤紫色の溶液となるので，570 nmにおける吸光度によって，ホルマザン産生量（＝ミトコンドリア酵素活性≒細胞生存率）を測定する。彼らの試験では，SWCNTsがMTTアッセイにあるテトラゾリウム塩と相互作用を示す知見を得ており，細胞生存活性を正しく評価できないことを主張している。

同様なことはIsobeらのカーボンナノホーンで行なった試験においても確認されている[30]。カーボンナノホーンは，単層のグラフィンシートが角のように円錐状に閉じたものの集合体であり，合成時に触媒を使用しないため，金属を一切含まない。彼らはアミンで化学修飾されたカーボンナノホーン凝集体に対して3T3細胞およびHeLa細胞の細胞生存率をMTTアッセイで行ったところ，アッセイで使用される芳香族染料の呈色を減少させ，誤ったデータを生じさせることを指摘している。このことは，MTTアッセイ，アラマーブルーアッセイ，ヨウ化プロピジウムアッセイのような染色に基づく細胞生存率の試験では色素に芳香族分子を使用しており，グラフィンで構成されているCNTsとの物理吸着の相互作用があり，一様に間違った結果を与える可能性を意味している。また，これまでにもCNTsは芳香族分子以外の分子も非特異性吸着する。このため，通常使われている酵素標識抗体法（Enzyme-Linked ImmunoSorbent Assay：ELISA）試験法がCNTsに適用できるか疑問が残る。

まったく違う観点からの実験であるが，Funbiらは精製MWCNTsに過酸化水素水やギ酸を加え，活性酸素発生実験において，MWCNTs分散液は活性酸素やラジカル種を発生させないこと，多くの水酸基活性ラジカルや活性酸素ラジカルを補足するという“スキャベンジャー効果”があることを見出しており[31]。CNTsが生体内でラジカル種を補足する効果により，免疫系のバランスを崩す可能性が起こりうることを指摘している。

現状では，ある1つの毒性試験を行なうことによりCNTsの安全性を完全に評価できるという決定的な方法はない。幾つかの試験を行い，相補的なデータを集めて，客観的に評価する地味な方法しかない。中でも時間を必要とする*in vivo* 試験は細胞・組織反応を評価するにはなくてはならない有効な毒性評価法である。筆者らはカルボキシル基で化学修飾されたMWCNTsのラット軟組織埋入試験を4週間行ったが，急性な炎症は観察されず[32]，現在は2年間の長期間の*in vivo* 試験を行っている最中である。アスベストのように発症するまでに長期間を必要とする症例を考慮すると，CNTsの長期間の*in vivo* 試験の必要性があると考える。

5 むすび

CNTsの表面と毒性について最近の論文を紹介した。CNTsの合成方法はたくさんあり，C_{60}のような分子量が決定されているわけでない。それゆえ，CNTsの評価法や標準化は非常に重要となってきている[33,34]。リスク評価に使用されるCNTsは，未精製CNTs，精製CNTs，化学修飾CNTsなどすべて詳細にキャラクタリゼーションされた共通なサンプルであるべきで，様々なリスク評価を行なうことにより，データベースを築き上げていくべきである。最近ではCNTsの標準化も検討されており，近い未来には，リスク評価においても均一なサンプルが提供され，試験が行なわれるのではないかと考える。

参考文献

1) 神山宣彦，セラミックス 29，111 (1994)

2) M. S. Dresselhaus, G. Dresselhaus and P. C. Eklund, *Science of Fullerenes and Carbon Nanotubes*, (Academic Press, San Diego, CA, 1996)

3) M. Uo, F. Watari, A. Yokoyama, H. Matsuno and T. Kawasaki, *Biomaterials* 22, 677 (2001)

4) A. Hoshino, K. Fujioka, T. Oku, M. Suga, Y. F. Sasaki, T. Ohta, M. Yasuhara, K. Suzuki and K. Yamamoto, *Nano Lett.* **4**, 2163 (2004)

5) E. E. Connor, E. E. Connor, J. Mwamuka, A. Gole, C. J. Murphy and M. D. Wyatt, *Small* 1, 325 (2005)

6) C. J. Johnston, J. N. Finkelstein, P. Mercer, N. Corson, R. Gelein and G. Oberdörster, *Toxicol. Appl. Pharmacol.* **168**, 208 (2000)

7) K. Tamura, N. Takashi, R. Kumazawa, F. Watari and Y. Totsuka, *Mater. Trans.* **43**, 3052 (2002)

8) R. Kumazawa, F. Watari, N. Takashi, Y. Tanimura, M. Uo and Y. Totsuka, *Biomaterials* 23, 3757 (2002)

9) M. Tsoli, H. Kuhn, W. Brandau, H. Esche and G. Schmid, *Small* 1, 841 (2005)

10) T. Kodama, *J. Stomatol. Soc. Jpn.* **38**, 263 (1989)

11) J. P. Landsberg, B. McDonald and F. Watt, *Nature* 360, 65 (1992)

12) J. L. Bard, J. R. Connor and B. C. Jones, *Nuter. Rev.* 51, 157 (1993)

13) M. A. Smith, P. L. R. Harris, L. M. Sayres and G. Perry, *Proc. Natl. Acad. Sci. USA* **94**, 9866 (1997)

14) F. Q. Shcafer, S. Y. Qian and G. R. Buettner, *Cell. Mol. Biol.* **46**, 657 (2000)

15) M. Layard, A. Tegeris, E. Miller, M. May, E. Morgan and A. Smith, *J. Natl. Cancer Inst.* **67**, 965 (1981)

16) F. Pott, *IARC Sci. Pub.* No. 30, Vol. 1, 286 (1980)

17) C. Journet and P. Bernier, *Appl. Phys. A* **67**, 1 (1998)

18) P. Dubruel, B. Christiaens, M. Rosseneu, J. Vandekerckhove, J. Grooten, V. Goossens and E. Schacht, *Biomacromolecules* 5, 379 (2004)

19) A. Aissaoui, N. Oudrhiri, L. Petit, M. Hauchecorne, E. Kan, M. Sainlos, S. Julia, J. Nacarro, J. P. Vigneron, J. M. Lehn and P. Lehn, *Curr. Drug Targets* **3**, 1 (2002)

20) N. A. Monteiro-Riviere, R. J. Nemanich, A. O. Inman, Y. Y. Wang and J. E. Riviere, *Toxicol. Lett.* **155**, 377 (2004)

21) J. Muller, F. Huaux, N. Moreau, P. Misson, J. -F. Heilier, M. Delos, M. Arras, A. Fonseca, J. B. Nagy and D. Lison, *Toxicol. Appl. Pharmacol.* **207**, 221 (2005)

22) IARC, *IARC Sci. Pub.* No. 97 (1990)

23) S. Koyama, M. Endo, Y. -A. Kim, T. Hayashi, T. Yanagisawa, K. Osaka, H. Koyama, H. Haniu and N. Kuroiwa, *Carbon* **44**, 1079 (2006)

24) C. M. Sayes, F. Liang, J. L. Hudson, J. Mendez, W. Guo, J. M. Beach, V. C. Moore, C. D. Doyle, J. L. West, W. E. Billups, K. D. Ausman and V. L. Colvin, *Toxicol. Lett* **161**, 135 (2006)

25) Q. Lu, J. M. Moore, G. Huang, A. S. Mount, A. M. Rao, L. L. Larcom and P. C. Ke, *Nano Lett.* **4**, 2473 (2004)

26) R. Singh, D. Pantarotto, L. Lacerda, G. Pastorin, C. Klumpp, M. Prato, A. Bianco and K. Kostarelos, *Proc. Natl. Acad. Sci. USA* **103**, 3357 (2006)

27) H. Dumortier, S. Lacotte, G. Pastorin, R. Marega, W. Wu, D. Bonifazi, J. -P. Briand, M. Prato, S. Muller and A. Bianco, *Nano Lett.* **6**, 1522 (2006)

28) K. Kostarelos, L. Lacerda, G. Pastorin, W. Wu, S. Wieckowski, J. Luangsivilay, S. Godefroy, D. Pantarotto, J. -P. Briand, S. Muller, M. Prato and A. Bianco, *Nat. Nanotech.* **2**, 108 (2007)

29) J. M. Wörle-Knirsch, K. Pulskamp and H. F. Krug, *Nano Lett.* **6**, 1261 (2006)

30) H. Isobe, T. Tanaka, R. Maeda, E. Noiri, N. Solin, M. Yudasaka, S.

Iijima and E. Nakamura, *Angew. Chem. Int. Edit.* **45**, 6676 (2006)

31) I. Fenoglio, M. Tomatis, D. Lison, J. Muller, A. Fonseca, J. B. Nagy and B. Fubini, *Free Radic. Biol. Med.* **40**, 1227 (2006)

32) Y. Sato, A. Yokoyama, K. -I. Shibata, Y. Akimoto, Y. Nodasaka, T. Kohgo, K. Tamura, T. Akasaka, M. Uo, K. Motomiya, B. Jeyadevan, M. Ishiguro, R. Hatakeyama, F. Watari and K. Tohji, *Mol. BioSyst.* **1**, 176 (2005)

33) http://www.msel.nist.gov/Nanotube2/Carbon_Nanotubes_Presentations.htm

34) http://www.inmetro.gov.br/msin07/program.asp

CARBON 46 (2008) 1927 1934

available at www.sciencedirect.com

ScienceDirect

journal homepage: www.elsevier.com/locate/carbon

Carbon

In vivo rat subcutaneous tissue response of binder-free multi-walled carbon nanotube blocks cross-linked by de-fluorination

Yoshinori Sato[a,], Atsuro Yokoyama[b,*], Takao Kasai[b], Shinji Hashiguchi[c], Makoto Ootsubo[a], Shin-ichi Ogino[a], Naoki Sashida[a], Masaru Namura[a], Kenichi Motomiya[a], Balachandran Jeyadevan[a], Kazuyuki Tohji[a]*

[a]*Graduate School of Environmental Studies, Tohoku University, Aoba 6-6-20, Aramaki, Aoba-ku, Sendai 980-8579, Japan*
[b]*Graduate School of Dental Medicine, Hokkaido University, Kita 13, Nishi 7, Kita-ku, Sapporo 060-8586, Japan*
[c]*Stella Chemifa Co., 1-41 Rinkai-cho, Izumiotsu, Osaka 595-0075, Japan*

ARTICLE INFO

Article history:
Received 22 May 2008
Accepted 2 August 2008
Available online 12 August 2008

ABSTRACT

Binder-free multi-walled carbon nanotube (MWCNT) blocks from fluorinated MWCNTs were prepared using thermal heating and a compression method in vacuo. The resulting carbon nanotube blocks are lighter than graphite, can be machined and polished, possess average bending strengths of 102.2 MPa, a bending modulus of 15.4 GPa, and moderate wettability. The binder-free MWCNT blocks possess good biocompatibility when tested in the subcutaneous tissue of rats in vivo, which were covered by thin granulation tissue, 40–70 μm in thickness, comprising a few lymphocytes, cell with large cytoplasmic spaces like fibroblasts and foreign-body giant cells. That is indicative of a slight inflammatory response than MWCNT/resin blocks and poly(methyl methacrylate). This material can potentially be employed as an alternative artificial hard tissue or internal bone plate that makes use of the properties of CNTs.

1. Introduction

Since the excellent antithrombotic property of graphite was discovered in 1963 [1], biocompatible artificial organs or internal bone plates have been developed using carbon materials such as low temperature isotropic carbon (LIT) [2,3] in high density isotropic carbon materials, carbon fiber-reinforced carbon composites (C/C) [4–8] and polymer/carbon fiber composites [9,10]. In particular, C/C have been used as an alternative hard tissue material of bone or dental root, which have been generated from carbon fibers (CFs) and resins by a combination of resin impregnation and hot press methods. Graphite and traditional C/C materials have been solidified by graphitization of a resin (binder) and possess an apparent density, 2.0–2.2 g/cm^3. Over the past several years, basic biomedical research concerning drug delivery [11–13] and the use of scaffolds [14–18] and catheters [19,20] has been carried out using a new type of carbon allotrope comprising carbon nanotubes (CNTs). We have investigated the use of alternative artificial hard tissue materials comprising CNT composites [21,22]. As CNTs possess low density, high mechanical strength [23] and protein adsorption properties [24,25], artificial hard tissue alternative materials comprising CNTs can potentially be utilized as lightweight, porous, and strong three-dimensional materials [26] composed of one-dimensional CNTs that offer advantages in comparison with the use of graphite and traditional C/C materials. Recently, we have produced large-sized binder-free multi-walled carbon

* *Corresponding authors:* Fax: +81 22 795 3868 (Y. Sato); +81 11 706 4903 (A. Yokoyama).
E-mail addresses: hige@bucky1.kankyo.tohoku.ac.jp (Y. Sato), yokoyama@den.hokudai.ac.jp (A. Yokoyama).
0008-6223/$ - see front matter
doi:10.1016/j.carbon.2008.08.003

nanotube (MWCNT) blocks from fluorinated MWCNTs using thermal heating and a compression method in vacuo (the blocks are referred to as "de-F-MWCNT blocks") [27]. This technique resulted in the formation of covalent MWCNT networks generated by the introduction of sp^3-hybridized carbon atoms that cross-link between nanotubes following de-fluorination. The resulting CNT blocks have a low apparent density 1.44 g/cm^3 derived from solidification of pure MWCNT in the absence of a binder, can be machined and polished, and possess average three times stronger mechanical strength, bending strengths of 102.2 MPa and a bending modulus of 15.4 GPa, than that of commercial graphite. Thus, the de-F-MWCNT blocks are light and strong, and can potentially be employed for use as alternative artificial hard tissue materials in biomedical application.

Biomaterials need to possess: (a) lightweight, mechanical strength, decay durability, abrasion-proof and fatigue-resistant properties and (b) antithrombogenicity, adhesion to body tissue, corrosion fatigue resistance and biocompatibility. The most critical factor concerns the biocompatibility of materials. Generally, use of the "implant test in vivo" [28], the most important and basic toxic evaluation method, is employed to examine material responses to tissue in vivo as well as cellular responsive reactions in vitro. Here, we report on the tissue response of binder-free de-F-MWCNT blocks following subcutaneous implant in rats to evaluate their biocompatibility comparing with MWCNT/resin blocks carbonized with 50 wt% phenol resin, poly(methyl methacrylate) (PMMA; negative control), and pure Ni metal (positive control) as reference materials.

2. Materials and methods

2.1. Purification of MWCNTs

The purity of the MWCNTs was ca. 80 wt%, and the rest of the material consisted of amorphous carbon (8.50 wt%), Al (5.73 wt%), Fe (4.43 wt%), Mo (1.27 wt%) and Cr (0.07 wt%). The nanotubes exhibited bamboo-like morphologies. The average tube diameter ranged from 20 to 40 nm, and the lengths ranged from 500 nm to 5.0 μm. The MWCNT soot was burned in air at 773 K for 90 min and the remaining soot was then introduced into a flask containing 6 M-HCl in order to dissolve the Fe, Mo and Cr. Following this procedure, the acid solution was filtered using a membrane filter, and 1.0 g of the filtered material was transferred into a flask with 1.0 L of 2 M-NaOH and refluxed at 373 K for 6 h in order to dissolve aluminum oxides. The resulting suspension was then filtered and washed with hot water. Finally, samples were dried in vacuo at 373 K for 24 h. Following purification, the impurities consisted of Na (0.40 wt%), Al (1.41 wt%), Fe (0.26 wt%), Mo (1.27 wt%) and Cr (0.15 wt%). The elemental analysis was obtained using inductively coupled plasma optical emission spectroscopy (ICP-OES).

2.2. Fluorination of MWCNTs

Purified MWCNTs (150 mg) were fluorinated at 523 K using a mixture of F_2 (20%) and N_2 (80%) for 2 h (flow rate of 25 mL/min). Thermal annealing was then carried out at 523 K for 6 h in a polytetrafluoroethylene cell under a nitrogen flow of 20 mL/min. We repeated this fluorination procedure several times. The products were then characterized by X-ray photoelectron spectroscopy (XPS) using an AXIS-His (Kratos Analytical Ltd., UK), and the C:F stoichiometries were determined.

2.3. Preparation of de-F-MWCNT blocks

The de-F-MWCNT blocks were prepared using a SPS system (Sumitomo Coal Mining, SPS-1050, Japan). The SPS systems is a unique synthesis and processing technique which allows for sintering at low temperatures and short periods of time by charging particles with electrical energy, and effectively applying the high energy of a spark plasma. The SPS process possesses very high thermal efficiency because of the direct heating caused by the spark, and can readily produce a homogeneous, high-quality sintered product due to the uniform heating generated. Typically, 300 mg of the MWCNT powder was used and hardened in a graphite mold with a diameter of 20 mm at 1273 K (heating rate: 25 K/min), under a pressure of 80 MPa in vacuo (1×10^{-2} Torr) for 10 min. The resulting sample was 20 mm in diameter and 2.0 mm in thickness. The typical weight loss of de-F-MWCNT blocks was 50.0–55.3 wt% of the initial fluorinated MWCNT powder.

2.4. Preparation of MWCNT/resin blocks

Purified MWCNTs (500 mg) was mixed with 500 mg of the phenol resin in 100 mL of ethanol at 298 K, sonicated for 1 h, and the ethanol was then evaporated at 333 K. Thermal annealing was then carried out at 773 K for 2 h in an alumina boat under a nitrogen flow of 20 mL/min in an effort to carbonize the phenol resin. In a similar manner as with the production of de-F-MWCNT blocks, 300 mg of the MWCNT powder was used and hardened in a graphite-covered die with a diameter of 20 mm at 1273 K (heating rate: 25 K/min), under a pressure of 80 MPa in vacuo (1×10^{-2} Torr) for 10 min. The resulting sample was 20 mm in diameter and ~2.0 mm in thickness. The weight loss of MWCNT/resin blocks was 5.0–10 wt% of the initial MWCNT/carbonized resin powder.

2.5. Analysis of materials

The sample morphologies were determined by scanning electron microscopy (SEM; S-4100, Hitachi, Japan) and high-resolution transmission electron microscopy (HRTEM; HF-2000, Hitachi, Japan) equipped with a field emission gun. SEM and HRTEM were operated at 5 and 200 kV, respectively. The HRTEM was equipped with a NORAN Instruments energy-dispersive X-ray detector and a Gatan imaging filter with an energy resolution of 1.0 eV. Metal impurities were detected by ICP-OES (Thermo elemental Co., Ltd., USA). The vibrational modes of the modified nanotube samples were characterized using Fourier transform-infrared absorption spectroscopy (FT-IR; Avatar 380, Thermo Electron Co., Ltd., USA). The samples were measured inside a KBr pellet. Water contact angles of the samples were measured using a contact angle meter (face CA-DS, Kyowa Interface Science Co., Ltd., Japan). The flaked particles from the sample blocks in distilled water were

measured using a particle counter (KL-27, RION Co., Ltd., Japan). For the contact angle and particle count measurements, the shape of the specimens tested was approximately $2.0 \times 1.0 \times 8$ mm. The blocks were polished with Emery paper (# 1200) and Fuji film lapping tape (# 2000 and # 4000) (Fuji Photo Film Co., Ltd., Japan). The mechanical properties of the solid blocks, the Young's modulus and fracture strength were measured using three-point bending tests, which were performed on a universal testing machine (Instron 5582) at atmospheric conditions and room temperature. The load was applied at a cross-head speed of 0.05 mm/min. The Young's modulus E_b and fracture strength σ_b were calculated as previously described. Three specimens were tested, and the averaged results were obtained. The shape of the specimens tested was approximately $2.0 \times 1.0 \times 18$ mm. The solid specimens were polished with Emery paper (# 1200) and Fuji film lapping tape (# 2000 and # 4000) (Fuji Photo Film Co., Ltd., Japan). Eight tests were performed on each material.

2.6. *Inflammatory response to MWCNT blocks and reference sample*

The shape of the de-F-MWCNT and MWCNT/resin blocks was $1.0 \times 1.0 \times 10$ mm, and that of PMMA and pure Ni metal (99.9%, Niraco Co., Japan) was $1.6 \times 1.9 \times 5.4$ and $0.7 \times 1.0 \times 6.6$ mm, respectively. All blocks were polished with Emery paper (# 1200) and Fuji film lapping tape (# 2000 and # 4000) (Fuji Photo Film Co., Ltd., Japan) and sonicated with distilled water to remove the polished powder. Six male 6-week-old Wistar strain rats were used in this study. Incisions were made bilaterally in the thoracic region under general anesthesia. Two pockets were made in the subcutaneous tissue. A block was implanted in the subcutaneous tissue in the thoracic region bilaterally in each rat. Animal experiments were performed in accordance with the Guide for the Care and Use of Laboratory Animals, Hokkaido University Graduate School of Dental Medicine. No rats were lost during the course of this study. Three numerical values were acquired for each condition.

2.7. *Histological procedure and observation by optical microscopy*

One week following surgery, segments of subcutaneous tissue including sample were excised, fixed and then embedded in paraffin. Hematoxylin and eosin-stained specimens were observed by optical microscopy (AX80, Olympus, Japan).

3. Results and discussion

The apparent density of the de-F-MWCNT blocks is 1.44 g/cm^3, and the fracture bending strength and Young's modulus (bending modulus) of the de-F-MWCNT blocks were on average 102.2 MPa (min 92.4 MPa, max 122.7 MPa) and 15.4 GPa, respectively (Table 1). The de-F-MWCNT blocks are light, possess excellent mechanical strength and are able to be manufactured and polished (Fig. 1a). The MWCNTs were found to be embedded in the whole cross-section (Fig. 1b). As can be seen on the fracture surface, each individual MWCNT was observed and seemed to have excellent contact along the nanotube axis. Other carbon materials were notably absent under the present conditions. The fracture bending strength and Young's modulus of the de-F-MWCNT blocks were 2.1 and 1.5 times larger, respectively, than those of MWCNT/resin blocks due to the cross-linking of each nanotube by de-fluorination [27].

Given that in biomaterials nanosize particles derived from abrasion, wear, or polish debris particles can cause inflammation [29–31], we measured a particle broken off from the de-F-MWCNT blocks immersed in distilled water (Fig. 2a). A particle analyzer is able to detect over 300 nm size particles. In the de-F-MWCNT blocks, particles were detected to be 11.9 (particle/mL) after 1 h and 8.7 (particle/mL) after 72 h, and demonstrating no difference with that of distilled water and PMMA. This indicates that there are few abrasions with particle sizes over 300 nm from the de-F-MWCNT blocks infiltrated in distilled water. Fig. 2b shows the contact angle of the sample for distilled water. Artificial blood vessels need to be antithrombogenic and show no protein adsorption. However, as artificial hard tissue alternative materials need to adhere closely to cells and tissues at the material interface, it is desirable that these materials possess hydrophilicity. The contact angle of the de-F-MWCNT blocks is 42.0°, which represents high hydrophilicity in comparison with that of PMMA. This indicates that the de-F-MWCNT blocks possess a suitable surface that could be utilized in artificial bone and dental root applications.

Soft tissue inflammatory responses to artificial materials are important at the early implantation stage. As time passes, the vicinity occupied by the artificial material is covered with granulation tissue comprising lymphocytes, cell with large cytoplasmic spaces like fibroblasts, macrophages, and fibroblasts that restore tissue grow vigorously with the onset of fibrosis. As more time passes, artificial materials are covered by a fibrous capsule. Therefore, the extent of the inflammatory response to artificial materials is indicated by the thickness of the granulation tissue, the number, type and distribution of polymorphonuclear leukocytes, lymphocytes, cell with large cytoplasmic spaces like fibroblasts, fibroblasts, foreign-body giant cells, and macrophages observed in the tissue [28]. Table 2 shows the thickness of the granulation tissue and cell types present in the granulation tissue at 1 week after surgery. Low- and high-magnification histological

Table 1 – Mechanical properties of CNT blocks

Characteristic	de-F-MWCNT blocks	MWCNT/resin blocks
Bulk density p (g/cm^3)	1.44	1.41
Youngs modulus E_b (GPa)	14.2–16.3	8.7–10.7
Fracture bending strength a_b (MPa)	92.4–123.0	41.2–56.1

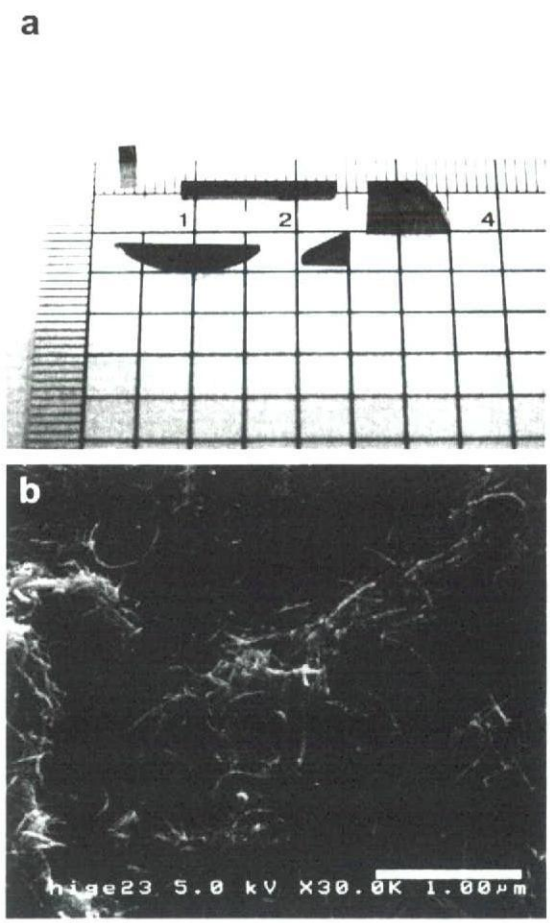

Fig. 1 – (a) Image showing variously shaped de-F-MWCNT blocks and (b) high-magnification SEM image of the fracture surface of the de-F-MWCNT blocks (scale bar; 1.0 μm).

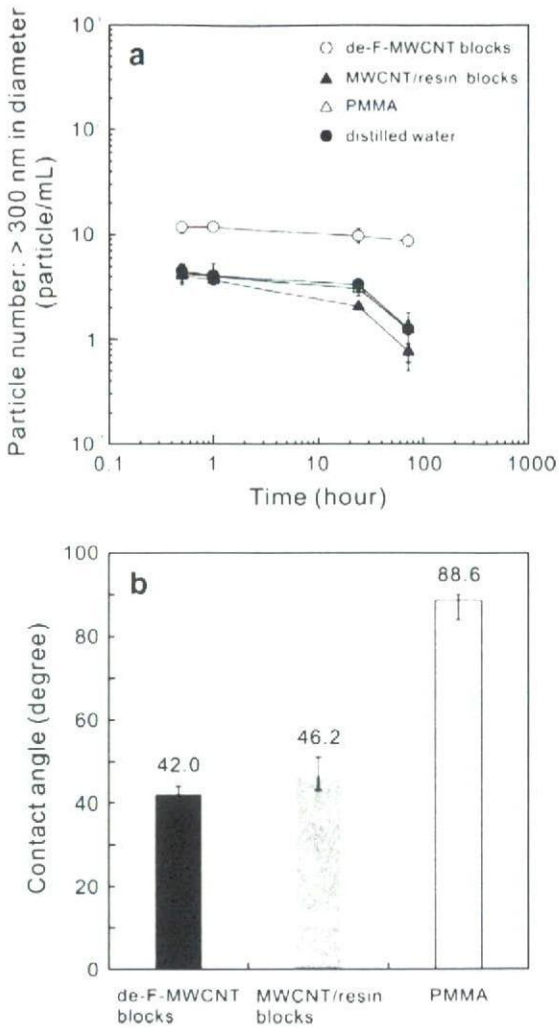

Fig. 2 – (a) Particle number (with size greater than 300 nm) from the samples infiltrated in distilled water as a function of time. de-F-MWCNT blocks (○), MWCNT/resin blocks (▲), and PMMA (△). The reference is distilled water. (b) Contact angle of sample for distilled water.

optical microscope images of each sample implanted in the subcutaneous tissue at 1 week after surgery are shown in Figs. 3 and 4. Asterisk (*) is the place where samples were implanted. The de-F-MWCNT blocks were covered by thin granulation tissue, 40–70 μm in thickness, comprising a few lymphocytes, cell with large cytoplasmic spaces like fibroblasts and foreign-body giant cells, which is indicative of a slight inflammatory response (Figs. 3 and 4a). On the other hand, in the MWCNT/resin blocks, a thick granulation tissue 290–340 μm in thickness was observed (Fig. 3b), comprising many lymphocytes, cell with large cytoplasmic spaces like fibroblasts and macrophages, in addition to dilatation of blood capillaries. This inflammation was greater than that observed with the de-F-MWCNT blocks. Macrophages and foreign-body giant cells positioned at the interface of the de-F-MWCNT blocks and MWCNT/resin blocks may be involved in the phagocytosis of a small number of less than 300 nm fragments detached from the blocks (Fig. 4b). The thickness of the granulation tissue surrounding PMMA was observed to be in the range between 40 and 120 μm (Fig. 3c), in which immature fibroblasts, macrophages, eosinophils and the dilatation of blood capillaries were observed (Fig. 4c). We found that the inflammation response to PMMA was moderately stronger than that of the de-F-MWCNT blocks, but weaker compared with that response observed for the MWCNT/resin blocks. The inflammatory response to the pure Ni metal positive control was strong, as indicated by the many macrophages, neutrophils, necrosed tissue (no nuclei, light pink color) and diapedesis of red blood cells that were observed (Figs. 3 and 4d) [32]. Thus, the de-F-MWCNT blocks were found to be associated with little acute inflammation and promising biocompatibility in the soft tissue given our examination of the thin granulation tissue. The biocompatibility of titanium [33] and hydroxyapatite [34] has been reported in terms of soft tissue responses in vivo with a view to establishing the efficacy of employing these biomaterials as bone supply materials and dental implants. Inflammatory responses to titanium and hydroxyapatite ceramics in soft tissue differ only slightly in comparison to the responses observed to de-F-MWCNT blocks, which are covered by thin fibrous connec-